Low-frequency self-pulsing in single-section quantum-dot laser diodes and its relation to optothermal pulsations

A. Tierno,[1] N. Radwell,[2] and T. Ackemann[3,*]

[1]*Université de Nice Sophia Antipolis, Institut Non-Linéaire de Nice, UMR 6618, F-06560 Valbonne, France*

[2]*SUPA and the School of Physics and Astronomy University of Glasgow, UK*

[3]*SUPA and the Department of Physics, University of Strathclyde, Glasgow G4 0NG, UK*

(Received 28 June 2011; published 17 October 2011)

Self-sustained pulsations in the output of an InAs quantum dot laser diode in the MHz range are reported. The characteristics (shape, range, and frequency) are presented for the free-running laser and when optical feedback in the Littrow configuration is applied. Bistability in the light-current characteristics is observed for operating wavelengths smaller than the gain peak, but it is not present for wavelengths above the gain peak and for the free-running laser, except at elevated temperatures. The temporal evolution of the envelopes of the optical spectra is very different for operation below, around, and above the gain peak, which might be related to a change of phase-amplitude coupling across the gain maximum, in agreement with the expectation for a two-level system. The time scale and the bifurcation scenario, supported by an initial blueshift of the emission wavelength of each longitudinal mode in time-resolved optical spectra, suggests that these are optothermal pulsations similar to those reported in quantum well amplifiers [Phys. Rev. E **68**, 036209 (2003)]. The mechanism of pulsation seems to be a destabilization of bistable states (due to saturable absorption in the beam wings) by a slow thermal change in the waveguiding properties.

DOI: 10.1103/PhysRevA.84.043828 PACS number(s): 42.55.Px, 42.60.Mi, 42.65.Sf, 85.30.−z

I. INTRODUCTION

Quantum dot (QD) lasers and amplifiers are emerging as an attractive light source in the wavelength range of 1.2–1.3 μm and it is important to assess their performance and stability (for a recent overview of the field see, e.g., the contributions in the special issues [1,2]). We recently reported investigations of a self-pulsing instability of quantum dot lasers in the MHz range [3,4]. Pulsations at a significantly higher (i.e., GHz) rate are very well known for quantum dot lasers [5–8]. The mechanism is self-Q-switching due to saturable absorption, and a pulsation period in the GHz region can be expected for passive Q switching with the lifetime of the excited state in the nanosecond range. In vertical-cavity surface-emitting lasers (VCSELs), self-pulsations were observed at a somewhat lower frequency, but still in the several hundreds of MHz range, and were related to saturable absorption in lateral unpumped regions of the device [9]. This mechanism for self-pulsations is known as the Yamada mechanism [10] for bulk and quantum well diodes. Self-pulsations in edge-emitting QD lasers without an intentionally introduced absorber section were also observed and explained in terms of the inhomogeneous nature of the QD gain, the existence of several confined QD states, and the resulting saturable absorption by energy states lower than the laser photon energy [11]. Nevertheless, these oscillations are still in the GHz range.

In the QD edge-emitting laser investigated here, self-pulsations take place without a saturable absorber section and on a MHz scale. The oscillation frequency as well as the square-wave shape hint of a thermal origin of the dynamics. Indeed, optothermal pulsations with a very similar phenomenology were studied in quantum well amplifiers [12,13] and are typical for a variety of other nonlinear optical systems [14–17]. It was shown in Ref. [12] that the self-oscillations follow van der Pol-Fitzhugh-Nagumo dynamics [18,19], a fairly general scenario of relaxation oscillations which are characterized by the competition of very different time scales (in Refs. [12,13], for example, carrier dynamics and thermal relaxation). In our case, the thermal time scale seems to be introduced by thermal lensing, which is strong enough to influence modal guiding due to the weakness of the built-in waveguide.

Interestingly, the self-pulsing dynamics are found to persist if frequency-selective feedback is applied. By the feedback, the operation frequency of the laser can be tuned above, below, and around gain maximum and time-resolved optical spectra show characteristic differences, which are argued to give some indication of a difference in phase-amplitude coupling above and below the gain maximum. For wavelengths below the gain peak the switch on of the laser with feedback is abrupt and shows a pronounced hysteresis, whereas the light-current characteristics (LI curve) is continuous and smooth for wavelengths higher than the gain peak and the free-running lasers. Again, optical bistability in quantum dot lasers is usually associated with two-section (i.e., gain and saturable absorption sections) laser structures displaying amplitude [5,20] or wavelength [21] bistability. The bistable operation has important applications in optical switching and modulation and is also well known for quantum well lasers [22]. Frequency-selective feedback is known also to support bistability at the lasing onset in single-section bulk and quantum well lasers [23,24].

This paper seeks to provide a comprehensive experimental investigation beyond the preliminary reports in conference proceedings [3,4] of what we consider to be an interesting instability, being potentially relevant for device design. The paper is organized as follows: In Sec. II, we describe the devices and the experimental setup. In Sec. III we give a

*thorsten.ackemann@strath.ac.uk

detailed characterization of the dynamics of the free-running laser and of the laser with feedback. A preliminary discussion suggests optothermal pulsations as the underlying mechanism of self-pulsation and will motivate the analysis of the time-resolved spectra. In Sec. IV, we then present a sampling method to obtain time-resolved optical spectra, which are analyzed on the level of single longitudinal modes and the spectral envelope. The section closes with a discussion of the level of temperature shifts and the resulting waveguiding dynamics within the structure.

II. DEVICES AND EXPERIMENTAL SETUP

The laser is a single-section edge-emitting diode (quantum dot laser, or QDL) from Innolume GmbH with a length of $L = 3.5$ mm. It contains ten layers of InAs QDs in a GaAs matrix. It is designed to have a single spatial mode with a shallow-edged waveguide and a stripe width of $w = 4.5\ \mu$m. One facet of the QDL diode is anti reflective (AR) coating while the other is high reflective (HR) coating. The laser is mounted on a C mount and the temperature is controlled by a Peltier element. The experimental setup is illustrated in Fig. 1. The emission in the fast axis is nearly collimated using a spherical lens C of 3.1 mm focal length and numerical aperture NA $= 0.68$. Feedback is provided in a Littrow scheme with a diffraction grating with 1450 lines/mm arranged at an angle $\Theta = 75^\circ$ with respect to the incoming beam. The collimator is positioned in a way to optimize threshold reduction by focusing on the grating (external cavity length 123 mm). After the external cavity, there are two lenses L1 and L2 for beam shaping and an optical isolator OI to prevent feedback from the detection part. Two InGaAs fast detectors (Thorlabs PDA255) with an active area of 1 mm^2 and a bandwidth of 50 MHz are used to monitor the dynamics of the total intensity and the spectrally resolved intensity after the scanning Fabry-Perot interferometer (SFP). The optical spectrum is also monitored by a commercial fiber-coupled optical spectrum analyzer

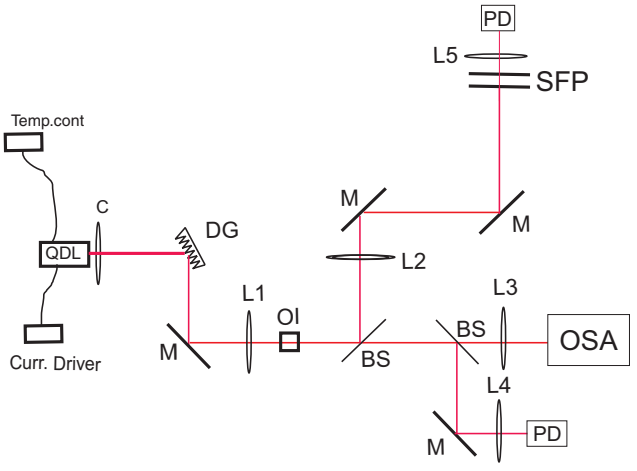

FIG. 1. (Color online) Experimental setup: quantum dot laser (QDL), aspheric collimator (C, $f = 3.1$ mm), diffraction grating (DG), mirror (M), L1 ($f = 100$ mm), optical isolator (OI), beam splitter (BS), L2 ($f = 250$ mm), scanning Fabry Perot interferometer (SFP), L3 ($f = 35$ mm), L4 ($f = 50$ mm), L5 ($f = 50$ mm), optical spectrum analyzer (OSA), photo diode (PD).

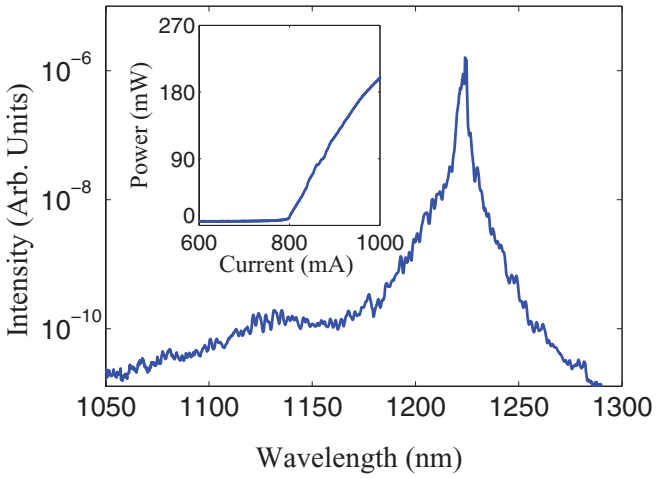

FIG. 2. (Color online) Lasing emission spectra of the QDL diode at $I = 810$ mA; inset shows time-averaged LI curve.

(Agilent 86140) with a nominal resolution of 0.07 nm. The plane-plane scanning Fabry-Perot interferometer (SFP) has a free spectral range of 1.95 nm (390 GHz) and a finesse of about 500 to 600. For the characterization of the free-running laser we simply replace the grating by a high-reflectivity mirror.

The investigations are based on two devices, showing qualitatively the same behavior, but the results shown are taken only from one laser. The threshold current of the free-running laser is $I = 760$ to 800 mA (see inset of Fig. 2), depending on temperature $T = 6$ to 10 °C. (The other device has a threshold current of $I = 850$ mA at $T = 10$ °C.) The emission wavelength is then centered around $\lambda = 1225$ nm; the exact value again being dependent on temperature and current. With feedback at the gain peak the threshold is reduced to $I = 550$ mA, a threshold reduction of about 27%. The relatively high threshold of the free-running lasers is due to the AR coating and the relatively weak guiding, which results in a low modal gain and possibly absorptive losses in the beam wings (as argued below). Two diodes with a better confinement (and a slightly longer cavity length of 4 mm), which do not show the self-pulsing instability described in this paper have thresholds in the range of 400–450 mA. Due to limited information from the grower and the sensitivity of the guiding, for weak guiding, to deviations from exactly rectangular geometries, we cannot quantify the difference in guiding conditions here.

Figure 2 show the lasing emission spectra for a current above threshold, $I = 810$ mA. It is possible to recognize two peaks corresponding to emission from the ground state (GS) and the first-excited state (ES1) of the QDs. The first excited state is localized at $\lambda = 1120$ nm, 100 nm away from the ground state at $\lambda = 1220$ nm where the lasing emission take place. Both GS and ES1 emission increase with increasing current until lasing emission takes place from the GS and the emission from ES1 remains constant over the investigated current range due to clamping of the carrier density. The LI curve shows a continuous onset of lasing emission and some saturation behavior at high current (see inset of Fig. 2).

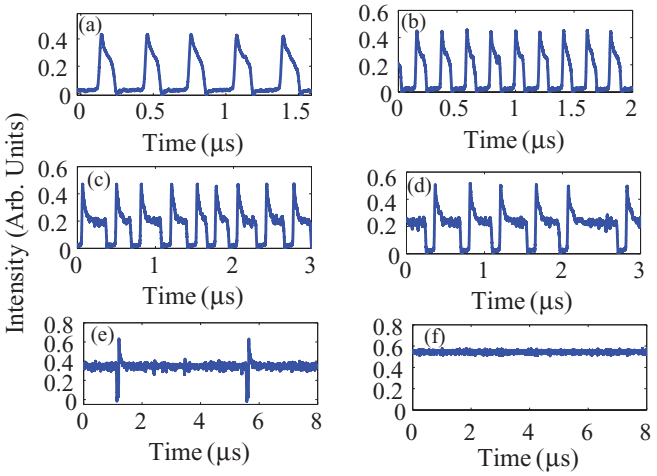

FIG. 3. (Color online) Behavior of the oscillation for the free-running laser for increasing current: (a) 803 mA, (b) 827 mA, (c) 832 mA, (d) 840 mA, (e) 872 mA, and (f) 910 mA.

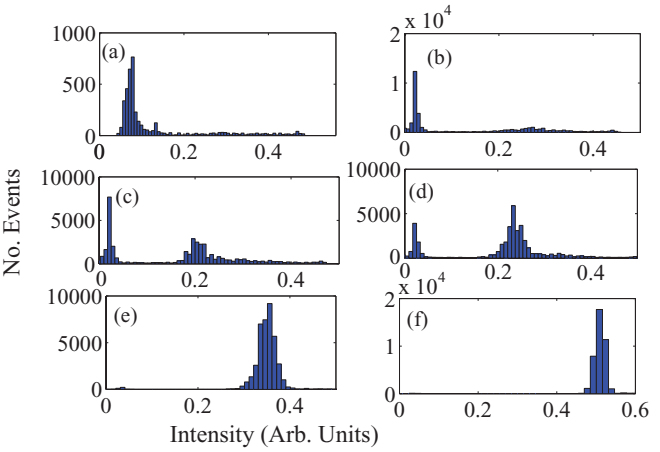

FIG. 4. (Color online) Histogram of amplitudes in time series for increasing current at: (a) 803 mA, (b) 827 mA, (c) 832 mA, (d) 840 mA, (e) 872 mA, and (f) 910 mA.

III. PHENOMENOLOGY OF SELF-PULSING

A. Experimental results: free-running laser

The QDL shows pronounced intensity pulsations (Fig. 3) starting at the threshold of the laser [Fig. 3(a)]. They are large-amplitude pulses on a small background. With increasing drive current their frequency increases and reaches a maximum characterized by approximately 50% duty cycle [Fig. 3(b)]. At higher currents, the on state dominates until the pulses are better described as short drop outs from a high-amplitude state [Figs. 3(d) and 3(e)].

The pulsations disappear after $I = 910$ mA and the laser emission is stable afterward [Fig. 3(f)]. The amplitude of the pulsations increases from low current to higher current, as evident from Figs. 3(a)–3(f).

It is evident from the figures that there is some variation in pulse duration [e.g., Figs. 3(c) and 3(d)]; that is, there is a jitter in the width of the pulses present at all drive currents.

The frequency of the pulsations is about 3 MHz around threshold current, which is 803 mA. It reaches 5 MHz [Fig. 3(b)] for $I = 827$ mA and decreases to 2 MHz at 840 mA [Fig. 3(d)] and then to less than 0.5 MHz for $I = 872$ mA [Fig. 3(e)]. At the boundary of the self-pulsing range, both at low and at high current, the pulses are very rare events; hence it is very difficult to have a detailed frequency analysis (see below, in discussion of Fig. 6).

The characteristics of the dynamics can be also illustrated by histograms of the intensity amplitudes for different current levels (Fig. 4). Figure 4(a) is obtained at $I = 803$ mA and demonstrates that the distribution of amplitudes is more concentrated around the base of the pulse, reflecting a spike-like behavior of the pulses. The fact that the distribution at high amplitude is broader than at low amplitudes is due to the overshoot at the start of the pulse. Figures 4(c) and 4(d), obtained at $I = 840$ mA, show a nearly evenly distributed frequency of occurrence of higher and lower intensity reflecting the approximately 50% duty cycle. For higher current, Fig. 4(e), there is a strong prevalence for the high-amplitude state with only some drops in power. Figure 4(f) illustrates the fluctuations of the laser amplitude in the stable range.

Figure 5 shows the histogram of peak amplitude (i.e., the peak value of the initial overshoot) for different current levels starting at laser threshold. The peak amplitude increases from low to high current; see Figs. 5(a)–5(e). The variation of the peak amplitude for the same current set is about 5%, without any apparent dependence on current, and is about the same as the fluctuations of the "dc" state, if the laser is stable; see Fig. 5(f).

The characteristics of the dynamics can also be illustrated by histograms of the time between pulses for different current levels [Figs. 6(a)–6(f)]. Figure 6(a) is obtained at the laser threshold, $I = 803$ mA, and demonstrates a symmetric distribution of interpulse times with a mean around 0.36 μs. The width of the distribution is about 0.03 μs (half width at half maximum, or HWHM) and corresponds to a jitter of the pulses. Increasing the current, the mean moves to

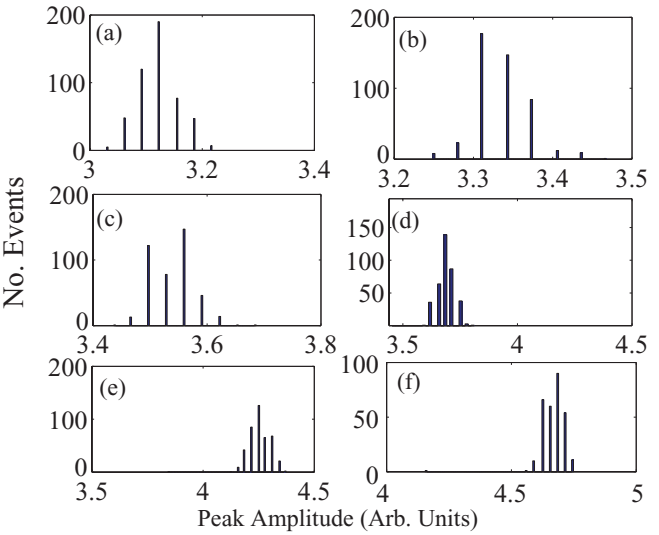

FIG. 5. (Color online) Histogram of the peak amplitude of pulses for increasing current at (a) 803 mA, (b) 827 mA, (c) 832 mA, (d) 840 mA, (e) 872 mA, and (f) 910 mA.

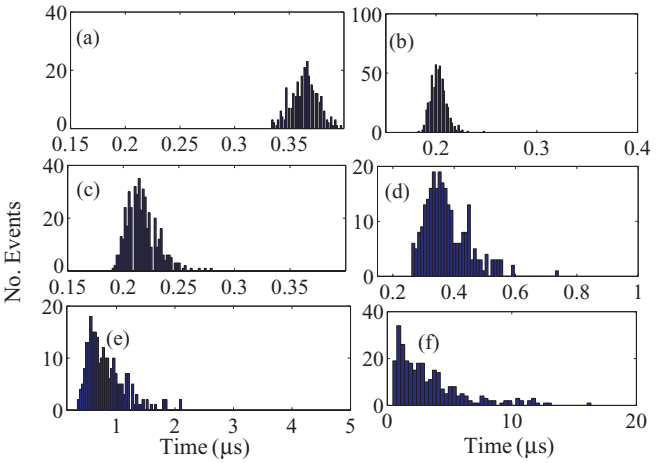

FIG. 6. (Color online) Interpulse-time histogram of the pulse for increasing current at (a) 803 mA, (b) 827 mA, (c) 832 mA, (d) 840 mA, (e) 872 mA, and (f) 890 mA.

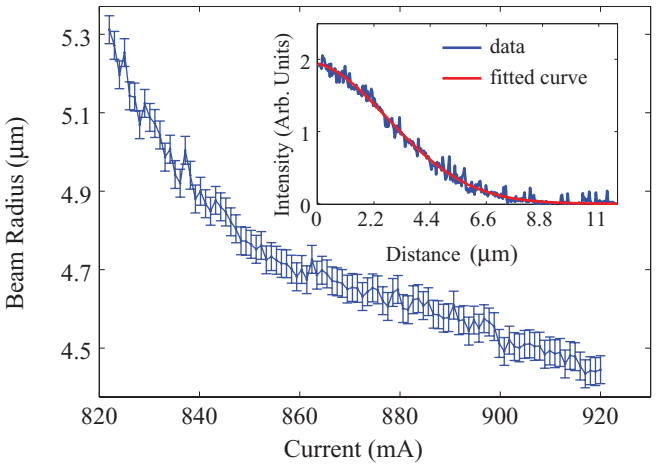

FIG. 7. (Color online) Time-averaged horizontal beam radius at the output facet of the laser as a function of current. The inset shows the profile (blue line) with a Gaussian fit (red line) at $I = 834$ mA. Laser threshold $I = 800$ mA.

0.2 μs [Fig. 6(b), $I = 827$ mA]; that is, the pulsations become more frequent, and the distribution narrows. For even higher current, the distributions become not only broader again, but also asymmetric [Figs. 6(c)–6(f)]. This means that the dynamics is most regular in the vicinity of the 50%-duty-cycle region and acquires more stochastic components afterward. The resulting variation in pulse duration is clearly visible. Figure 6(f) extends to 20 μs (i.e., there can be very rare events).

B. Beam profile and temperature dependence

Since the observed fairly low pulsation frequency suggest a possible contribution by thermal effects, we investigate the influence of current-induced heating and a change of the ambient temperature. First, we turn our attention to the beam-profile dependence on current. The intensity distribution at the exit facet of the diode is imaged into an InGaAs camera at a distance of $d = 1660$ mm from the collimating lens (magnification 535.5). Figure 7 shows the beam radius ($1/e^2$ point of intensity) along the slow axis of the QDL as a function of current. The profiles are Gaussian to a good approximation (see inset). The beam width decreases with increasing current from 5.3 μm at $I = 820$ mA to 4.4 μm at $I = 920$ mA, whereas the beam size along the fast axis is constant (not shown).

In addition, LI curves were taken at different temperatures including quite elevated temperatures. Figure 8 shows time-averaged LI curves of a self-pulsing diode (laser threshold $I = 526$ mA at 6 °C) for different temperatures. The curves for low temperatures show a lower threshold than reported before (e.g., Fig. 2); that is, the threshold current had dropped as we resumed investigations for Fig. 8 in the course of the investigations, possibly due to some aging effect. However, we stress that the data in Fig. 8 represent again a robust and stable behavior. Below 44 °C there is a continuous onset of lasing emission, although the initial part of the LI curve is quite steep. At a second kink, the slope becomes again smaller. Pulsations exist between threshold and this second kink (circular data points in the inset of Fig. 8). Within the self-pulsing region, the behavior is qualitative, the same as reported in Fig. 3. This upper limit increases more slowly with temperature than the threshold and hence the range with pulsations decreases.

At high temperature (above 50 °C) the pulsations are not present anymore and the switch on of the laser becomes abrupt displaying hysteresis (i.e., the laser becomes bistable). The width of the hysteresis loop increases with temperature. The LI curve at 44 °C represents the transition. A similar transition from pulsed (mode-locked in their case) operation to bistability was observed in two-section QD lasers [25] and might be related to a decrease of absorption recovery time and hence an increase in saturation power with temperature [26]. In general,

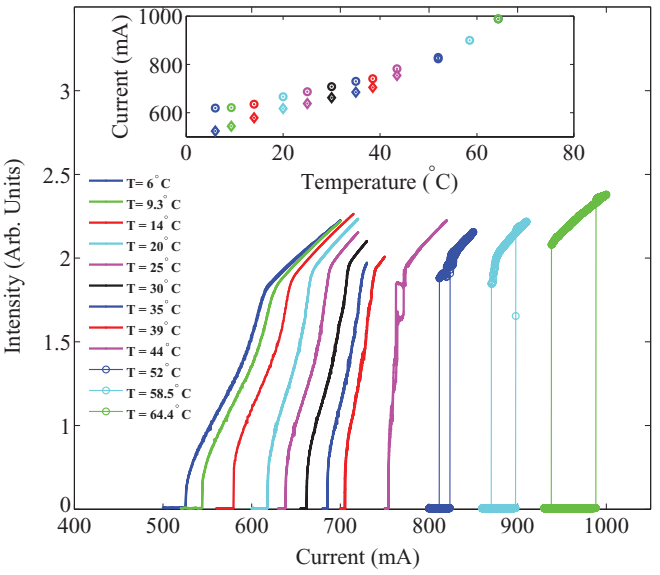

FIG. 8. (Color online) Time-averaged LI curves for different temperature (temperature increasing from left to right curves). The inset shows the threshold (diamonds) and the end of the oscillation range (circles) as a function of temperature.

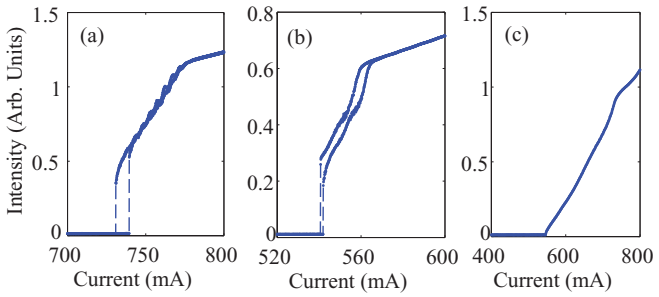

FIG. 9. (Color online) Time-averaged LI curves at (a) $\lambda = 1195$ nm, (b) gain peak, $\lambda = 1221$ nm, and (c) $\lambda = 1240$ nm.

a close connection between self-pulsing and bistability is well known for saturable absorber dynamics [5,22].

C. Experimental results: feedback

The laser with feedback also shows pulsations. They appear at frequencies somewhat lower than those in the free-running laser and are centered around 1 MHz. The qualitative behavior of the pulsations does not depend on wavelength and is quite the same as in the free-running laser: Short pulses from an off state evolve towards a 50% duty cycle. Then the on phases become longer until the laser is stable at high currents. Between 1195 and 1220 nm, the range where the oscillations are present is quite small, around 40 mA, then it increases to around 100 mA around the central wavelength to increase again up to 200 mA for higher wavelengths. Details are reported in Ref. [4].

Measurement of time-averaged LI curves at low temperatures have been taken by scanning the current of the laser in steps of 0.1 mA, which is the resolution of our current driver, up and down. The time-averaged LI curves differ strongly below the wavelength of minimal threshold of 1230 nm and above. At $\lambda = 1195$ nm [Fig. 9(a)], there is bistability at the laser threshold with a pronounced hysteresis loop. Afterwards, the average intensity increases linearly. At a kink at about 780 mA the slope of the LI curve changes and the laser becomes stable. Increasing the emission wavelength, the width of the hysteresis loop becomes smaller but an abrupt transition is still present up to $\lambda = 1221$ nm [Fig. 9(b)]. Figure 9(c) refers to $\lambda = 1240$ nm where there is no sign of bistability and the laser threshold is continuous.

Figures 9(a) and 9(b) shows some ripples in the LI curve just above the point where the curve became linear and which are not present for the free-running lasers at wavelengths above the gain peak. The repetition rate of these ripple is about 4.8 mA for $\lambda = 1195$ nm, but not present for $\lambda = 1221$ nm where, also after the switch on, there is no overlap between the two sides of the LI curve. Assuming that the ripples are caused by some interference effect where the phase changes due to the wavelength change due the current-induced ohmic heating in the diodes, one could infer a corresponding spectral shift. Unfortunately, the latter wavelength is not easy to measure due to the multimode and unstable behavior of the diode but our best estimation is about 0.0048 nm/mA. This results in a spectral period of 0.023 nm or 5 GHz, which is about half the FSR of the diode. Hence the origin of the modulation is currently not clear.

D. Discussion

First, we note again that we did not observe indications for higher QD state lasing, (Fig. 2), as in Ref. [11] and the frequency of self-pulsing is in the MHz instead of the GHz range. The slow time scale of these oscillation indicates that these are optothermal pulsations. Optothermal pulsations are a common scenario in broad-area semiconductor (quantum well) optical amplifiers, although at slightly slower time scales of kHz to hundreds of kHz [12,13]. The described phenomenology of pulsing from a low-amplitude state via 50% duty cycle to drop-outs from a high-amplitude state is found to be nearly identically in both systems. In the amplifier, the scenario can be dynamically interpreted within the scenario of the van der Pol-Fitzugh-Nagumo model [18,19] of interaction of dynamics at two very different time scales. In physical terms, there is a competition between two frequencies or resonances (e.g., in a laser with injection, the frequency of the injected light and the cavity resonance of the slave).

Initially they might be in resonance but, if amplification then sets in, the slave cools due to the reduction in carrier density due to stimulated emission, its resonance shifts, and interaction is lost. Then the carrier density is high again and the laser heats until it is in resonance again and a new pulse can start. The different time scales of thermal heating, respectively cooling, and stimulated emission as well as carrier injection lead then to relaxation-oscillation-like pulsations.

The difference between our case and the previous cases cited in the literature is the fact that, in our case, these oscillations appear also in the free-running laser. This indicates that the laser itself provides a mechanism which is able to generate oscillations in the MHz range. As indicated in the introduction, self-Q-switching without an explicit absorber section relying on saturable absorption in the beam wings is a possible mechanism for self-pulsations in single-section lasers and the dynamics might be slower than for two-section lasers because carrier diffusion plays a role. However, it is usually still in the hundreds of MHz range (see Ref. [9] for QD VCSELs). The classical analysis by Yamada in Ref. [10] for ridge-waveguide lasers gives about 300 MHz for the lowest numerical value and 600 MHz for the lowest repetition rate observed experimentally. In addition, the frequency is monotonic with current, as are the usual laser relaxation oscillations (closely related to self-Q-switching). This is in strong disagreement with our observation.

Another alternative mechanism known to enable self-pulsations in single-section lasers is spatial hole burning (SHB) [27]. However, Ref. [27] also reports a monotonic increase of pulsing frequency with current whereas we see a strongly nonmonotonic behavior and the pulsations frequencies are larger than 1 GHz. Apart from self-pulsing, one might envisage erratic or deterministic switching between different longitudinal modes (or groups of modes) due to the saturation effects of the standing waves inside the laser medium but this is not what we see. Either a multitude of longitudinal modes is on or the laser is off, as we will see in the next section.

Spatially resolved measurements yielded differences between the dynamics in the device center and beam wings: The initial overshoot at switch on takes place at beam center [28]. In addition, the time-averaged beam radius becomes smaller

for increasing current. This indicates a contribution of thermal lensing or waveguiding in maintaining the pulsations. Due to the shallow etching, the mode is not strongly confined but the confinement is enhanced by the refractive index increase in the ridge due to Joule heating. This enhances modal gain as well as reduces losses in the beam wings extending to unpumped regions. After switch on, radiative cooling leads to a reduction in confinement and the laser switches down again. Then the process is started again by heating. At some point, the average heat load is high enough to induce a thermal lens strong enough to sustain cw lasing. The relationship between temporal (τ) and spatial (s) scales for diffusive processes (diffusion constant D) and is roughly given by $\tau = s^2/D$ (see also Ref. [29] for specific geometries). Taking the width of the ridge-waveguide as a typical length scale, $s = 5\ \mu$m, and a thermal diffusivity of GaAs of $D = 2.5 \times 10^{-5}$ to 1.3×10^{-4} m^2/s [30,31], one obtains $\tau = 0.2$ to $1\ \mu$s, in good agreement with observation.

These arguments explain the mechanism of pulsation, but to explain the abrupt transition and the square-wave shape of the pulses an additional ingredient is necessary. Indeed it is a special feature of the Fitzugh-Nagumo model [18,19] that it relates bistability and large-amplitude square-wave-like self-pulsing. Bistable states resulting from fast dynamics (here carrier dynamics) are destabilized on long time scales by thermal effects changing the parameters of the fast dynamics. During this long lethargic period the amplitude is essentially constant until the range of stability is left and a fast transition to the other bistable state takes place. Here, the change in beam size changes modal gain and losses and hence the stability of the on and off states given by the relative values of modal gain and losses. Saturable losses in the beam wings (cf. the discussion of the Yamada model above) give the possibility of fast, abrupt transitions. The close connection between self-pulsing and bistability has been known for a long time for saturable absorption [5,22]. Since we find bistability in our lasers in some free-running and feedback-parameter conditions, the notion of self-pulsation due to thermal perturbations of bistable states seems to be plausible.

In the next section, we look at time-resolved spectra to obtain a better understanding of the dynamics and, in particular, to check for a direct indication for a transient temperature shift during the pulse.

IV. TIME-RESOLVED SPECTRA

A. Experimental scheme and results

Figure 10 shows standard time-averaged optical spectra (i.e., the sweeping time of the SFP is much longer than the time scale of pulsations) for the QDL with feedback operating around the gain peak ($\lambda = 1220$ nm, temperature $T = 15\,^{\circ}$C).

The spectrum in the upper part, Fig. 10(a), corresponds to stable operation of the laser, whereas the laser exhibits pulsations in the case of the lower panel, Fig. 10(b). In both cases, the laser is strongly multimode covering about 1.5 nm. The modal envelope is increasing from lower to higher wavelengths. For stable emission, individual longitudinal modes are clearly resolved (the free spectral range of the QDL is 11.6 GHz or 0.06 nm). The linewidth of an individual longitudinal mode is about 0.6 GHz (possibly resolution limited). Instead, when

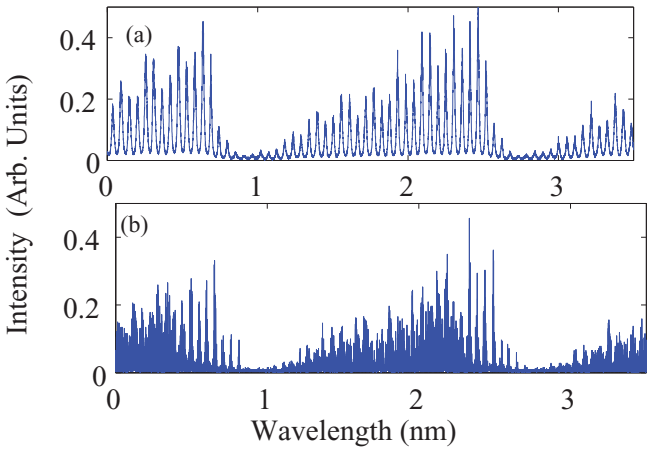

FIG. 10. (Color online) Time-averaged spectra of the laser with feedback for two relevant currents: (a) laser stable at $I = 584$ mA, (b) laser oscillating at $I = 548$ mA. The wavelength scale is only relative, the free spectral range of the analyzing SFP is 1.95 nm (i.e., the repetition of modes is a detection artifact).

pulsating, the average linewidth is larger [Fig. 10(b)], about 5.6 GHz, which might be due to modes jittering.

Following [32], we then record the time-resolved spectrum for all frequencies inside a free spectral range and superimpose the data recorded for every frequency. This is done by scanning the piezoelectric translators of the SFP by a computer-controlled voltage slowly (stepwise) while we record with a fast detector the signal transmitted by the SFP. The diode drive current is kept fixed during the experiment. To maintain a stable signal on the scope we trigger on the pulse read out by the other fast detector (without spectral resolution). In our case, a free spectral range of the SFP (1.95 nm) can be scanned by 0.47 V from the data acquisition (DAQ) card [amplified afterward with a high-voltage (HV) amplifier]. The scan covers 0.8 V with a resolution of 1 mV steps leading to coverage of almost two FSR with a nominal wavelength resolution of 0.0041 nm or 0.82 GHz. The validity of this

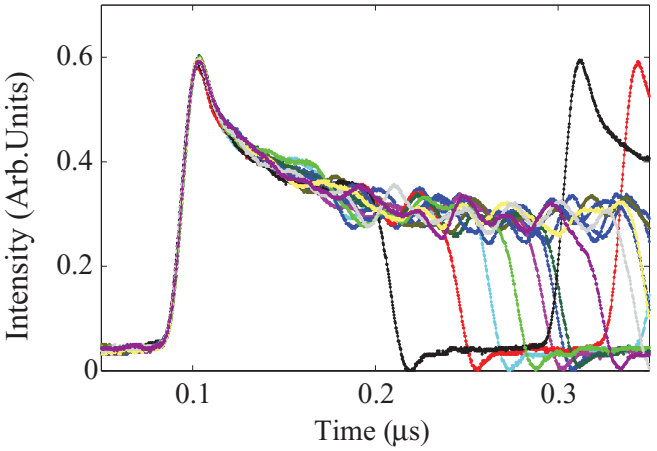

FIG. 11. (Color online) Superpositions of typical pulse shapes obtained by a non-frequency-selective monitor illustrating the timing jitter. The results are reliable in the first 0.2 μs (i.e., the interesting interval during the overshoot), whereas the jitter of pulse duration affects the reproducibility later on.

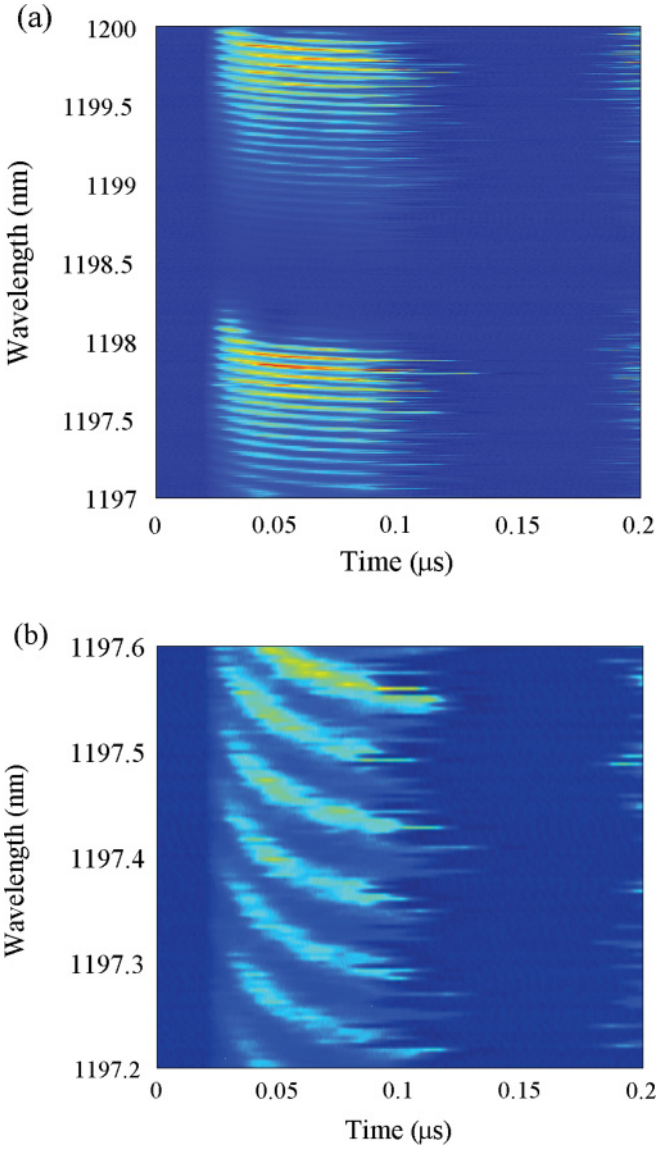

FIG. 12. (Color online) (a) Time-resolved spectrum of the laser with feedback for $\lambda = 1197$ nm, $I = 724$ mA. (b) Zoom of (a) from $\lambda = 1197.2$ nm to $\lambda = 1197.4$ nm. The repetition of the modal groups in (a) is again an artifact of the free spectral range of the analyzing SFP. A constant offset is added to the relative wavelength scale given by the piezo voltage in order to allow for an easy distinction between the different cases shown in Figs. 12–14. The absolute wavelength is not accurate.

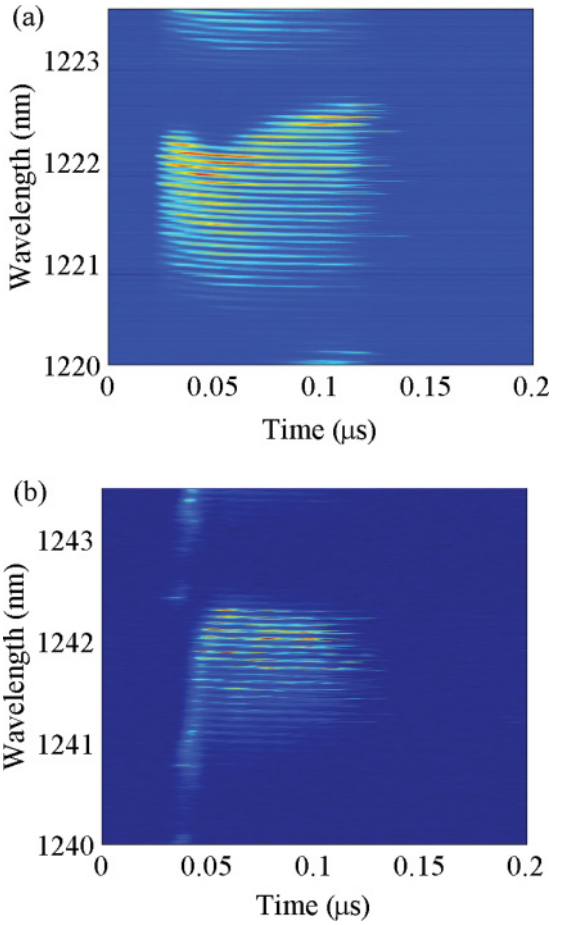

FIG. 13. (Color online) Time-resolved spectrum of laser with feedback for (a) $\lambda = 1221$ nm at $I = 548$ mA, (b) $\lambda = 1240$ nm at $I = 600$ mA.

sampling approach is demonstrated in Fig. 11, which shows typical examples of triggered pulses. The interesting initial phase is faithfully reproduced but, for longer times, the timing jitter breaks the reproducibility.

Figure 12 shows the time-resolved spectra for a wavelength of $\lambda = 1197$ nm at $I = 724$ mA, almost at the low-wavelength edge of the tuning range achievable tuning the diffraction grating. The trajectory of each longitudinal mode is initially curved (blueshifting) until it remains essentially constant for the remainder of the pulse, Fig. 12(b). This blueshift covers about 0.13 nm and might be due to radiative cooling. In addition, the lasing envelope also shifts, the blueish modes being excited and dying first, whereas the reddish modes switch on later and stay on until the end of the pulse. There is always a multitude of modes excited.

Figure 13(a) is for $\lambda = 1220$ nm, around the gain peak, at $I = 548$ mA. Again the envelope blueshifts in the initial phase, although it is less pronounced at $\lambda = 1197$ nm, but then swings back toward the red. Within each cavity mode there is a blueshift of 0.11 nm. Figure 13(b) is for $\lambda = 1240$ nm at $I = 600$ mA. In this case, the lasing starts at low wavelengths and then the envelope strongly redshifts. Within each cavity mode there is a blueshift of 0.06 nm.

Figure 14(a) shows instead the time-resolved spectrum for the free-running laser at a typical current. The spectral envelope is broader without the frequency filter in the feedback loop and hence the FSR of the analyzing SFP was increased to 5.7 nm (i.e., the spectral resolution is a factor of 3 lower). In the free-running-laser case there is a very weak blueshift of 0.02 nm for each longitudinal mode [Fig. 14(b)] but the envelope does not shift very much. The fact that the diagram is quite jagged for longer times is related to the fact that there is a larger dispersion of pulse length in the free-running laser than in the laser with feedback, which makes the sampling technique less reliable further away from the trigger point.

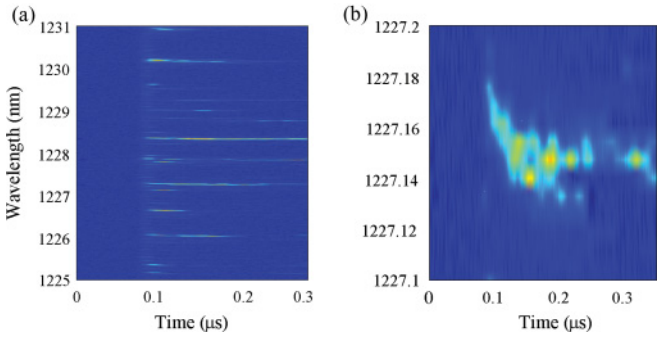

FIG. 14. (Color online) (a) Time-resolved spectrum for the free-running laser at $I = 831$ mA ($\lambda = 1225$ nm). The FSR of the analyzing SFP was increased to 5.7 nm. (b) Blow-up for one longitudinal mode.

B. Discussion

Switching between longitudinal modes was discussed in [33–36] for quantum well lasers and in Ref. [37] for quantum dot lasers. An important conclusion was that longitudinal mode switching is not merely a stochastic process but follows a quite deterministic switching sequence influenced by nonlinearities. A preference for a switching sequence from blue to red modes was related to the breaking of the symmetry of four-wave mixing processes by a nonzero α factor. The α factor or linewidth-enhancement factor describes phase-amplitude coupling in semiconductors and is positive for quantum well samples [38]. It is related to the fact that the gain spectrum (imaginary part of susceptibility) of quantum wells is asymmetric and, as a consequence, its Hilbert transform giving the contribution of the real part (refractive index) is not zero at the gain maximum. A positive α factor was found to be consistent with the blue-to-red switching sequence observed [34,36]. The three-dimensional (3D) quantum confinement of an ideal QD should lead to a "quasi-atomic" behavior with a delta-function-like density of states. A symmetric gain spectrum should have zero phase-amplitude coupling or linewidth-enhancement factor at the gain maximum; positive for lower frequencies and negative for higher frequencies. The different shift of the longitudinal modes during the pulses observed is in qualitative agreement with this expectation: On the gain maximum, the free-running laser as well as the laser with feedback do not show much of a shift consistent with a zero or small α factor. The detuned emission under frequency-selective feedback shows the same tendency as the quantum well devices for lower frequencies (positive α factor) and the opposite for higher frequencies (negative α factor). The size and sign of the α factor is very important for feedback and filamentation instabilities. Indeed, a reduced (or even negative) α factor and a reduced tendency to beam filamentation was observed in many QD samples, at least under some operating conditions [39–43]. The real susceptibility of QDs is more complicated than that of a two-level atom due to contributions from the wetting layer, higher QD states, and inhomogeneous broadening (see, e.g., Ref. [44]), although the possibility of a negative α factor under gain conditions can survive. The current observation of a qualitative agreement with the two-level expectation seems to be interesting, although it should be cautioned that the argument is quite indirect.

Bistability in single-longitudinal-mode quantum well lasers with narrow-band frequency-selective feedback arises due to the fact that phase-amplitude coupling can compensate for a detuning between cavity resonance and filter frequency; that is, the redshift (for positive α factor) of the cavity resonance due to the decrease in carrier density if the laser power increases can lead to an alignment of the cavity resonance with the feedback frequency even if they are initially misaligned. This can lead to an abrupt switch on of the laser with hysteresis at threshold [23,24] and to bistability between different longitudinal modes above threshold [45–47]. Since the feedback supports multiple longitudinal modes here, this mechanism is probably not applicable. In addition, the sign of the α factor as argued above from the shift of the modal envelopes for emission wavelengths lower than the gain peak is opposite to the one for quantum well lasers. This indicates that the origin of bistability is probably not dispersive (i.e., it is not related to refractive index effects) but due the saturation of losses. We argued before at the end of Sec. III D that parts of the beam experience saturable absorption in unpumped regions due to weak confinement. The relative influence might increase with decreasing wavelength because the tails of the contribution of the excited state to the susceptibility becomes more important.

Finally, the fact that each longitudinal mode blueshifts at the beginning of the pulse hints to a detuning-independent effect like a temperature shift. A blueshift is consistent with radiative cooling, which might trigger the thermal relaxation oscillations. This would fit the interpretation in the amplifier systems [12,13] where it was not explicitly demonstrated experimentally. The depletion of carrier density during the turn-on transient might influence the shift on a quantitative level (i.e., be responsible for the differences for the different emission wavelengths). For wavelengths above the gain maximum, $\alpha < 0$ in the two-level approximation, which results in a blueshift with depleting carriers. For wavelengths below the gain maximum, $\alpha > 0$ in the two-level approximation, which results in a redshift with depleting carriers. This actually fits with the observed decrease in the shift with increasing wavelength, although it does not explain the small shift in the free-running laser. The latter might be related to the fact that the threshold and thus carrier density is much higher in the latter than with feedback. Under conditions of high carrier density it is fairly well established that the α factor can be significantly larger than zero due to contributions from the excited states and the wetting layer [42–44], leading to a larger redshift possibly compensating the temperature-induced blueshift. Note that the assumption of a carrier-induced effect based on a positive α factor alone (i.e., dominated by the excited states and wetting layer susceptibility) would lead to the prediction of a redshift, in strong disagreement with our observation.

The thermal tuning of the cavity modes in these QDL structures is about 0.1 nm/K, indicating temperature changes in the range of 0.2 to 1.3 K, if the initial shift is related to radiative cooling. Assuming the one-dimensional theory for simple rectangularly shaped dielectric waveguides the observed change of beam radius in Fig. 7 is compatible with a change of the effective index difference between core and cladding of $\pm 1.5 \times 10^{-4}$ around the estimated effective index

difference of 0.001. Since the thermal change of the refractive index of GaAs is about 2×10^{-4}/K, only a very small temperature difference between the center of the waveguide and the surrounding is needed to influence waveguiding significantly (i.e., it seems to be very feasible that a thermal lens induced by the Joule heating in the center of the waveguide provides this increased lateral confinement of the mode). Note that the overall thermal heating by current is obviously much higher than a degree or so, for the considerations here it is sufficient that the current heating—being centered in the ridge—is likely to produce also a small differential between the center and the tails of the ridge. Hence the proposed explanation seems to be self-consistent.

V. CONCLUSION

Self-sustained pulsations of the output have been observed in a InAs quantum dot laser diodes in the MHz range. The pulsations tend toward a square-wave-like appearance and are present for a wide range of current and wavelength. Optical bistability is also found, although no saturable section is included, and is probably due to saturable absorption in the beam wings. The time scale and the bifurcation scenario suggest that these are optothermal pulsations similar to those reported in quantum well amplifiers [12], but there is no obvious mechanism of competition between resonance conditions. Instead, we propose the hypothesis of a dynamical change of thermal waveguiding properties. Due to the weak intrinsic guiding, changes in thermal guiding are relevant and interact on a slow time scale with the faster (gain as well as absorptive) carrier dynamics.

The interpretation of the initial blueshift in the time-resolved spectra as radiative cooling seems to be consisting with the observations, especially the α factor of QD. However, we consider the experimental results to be interesting in there own right and to be potentially relevant for device design, independent of the details of the interpretation. Obviously, this paper provides only a phenomenological description of the instability. It would be helpful to have a dynamical model which enables one to address the different contributions from gain dynamics, saturable absorption, phase-amplitude coupling, and waveguiding and study the transition between bistable and self-pulsing operations, but this is of significant complexity and beyond the scope of the present work.

ACKNOWLEDGMENTS

This work was supported by EPSRC project EP/E025021. A.T. gratefully acknowledges funding of Région Provence Alpes Cote d'Azur (DEB 10-924). We are grateful for useful discussions with D. Livshits from Innolume GmbH, S. Barland, and A.M. Yacomotti. The experimental investigations were performed when the authors were at the University of Strathclyde.

[1] P. Bhattacharya, D. Bimberg, and Y. Arakawa, Proc. IEEE **95**, 1718 (2007).
[2] M. Sugawara and M. Usami, Nature Phot. **3**, 30 (2009).
[3] A. Tierno, N. Radwell, and T. Ackemann, Proc. SPIE **7720**, 77202H (2010).
[4] A. Tierno and T. Ackemann, J. Phys.: Conf. Ser. **245**, 012092 (2010).
[5] O. Qasaimeh, W.-D. Zhou, J. Phillips, S. Krishna, P. Bhattacharyaa, and M. Dutta, Appl. Phys. Lett. **74**, 1654 (1999).
[6] H. D. Summers, D. R. Matthews, P. M. Smowton, P. Rees, and M. Hopkinson, J. Appl. Phys. **95**, 1036 (2004).
[7] E. A. Viktorov, M. A. Cataluna, L. O Faolain, T. F. Krauss, W. Sibbett, E. U. Rafailov, and P. Mandela, Appl. Phys. Lett. **90**, 121113 (2007).
[8] H. Liu, P. Smowton, H. Summers, G. Edwards, and W. Drexler, Appl. Phys. Lett. **95**, 101111 (2009).
[9] A. G. Kuzmenkov *et al.*, Appl. Phys. Lett. **91**, 121106 (2007).
[10] M. Yamada, IEEE J. Quantum Electron. **29**, 1330 (1993).
[11] S. Mokkapati, H. H. Tan, C. Jagadish, and M. Buda, Appl. Phys. Lett. **92**, 021104 (2008).
[12] S. Barland, O. Piro, M. Giudici, J. R. Tredicce, and S. Balle, Phys. Rev. E **68**, 036209 (2003).
[13] F. Marino, G. Catalán, P. Sánchez, S. Balle, and O. Piro, Phys. Rev. Lett. **92**, 073901 (2004).
[14] M. Wegener and C. Klingshirn, Phys. Rev. A **35**, 1740 (1987).
[15] Y. A. Rzhanov, H. Richardson, A. A. Hagberg, and J. V. Moloney, Phys. Rev. A **47**, 1480 (1993).
[16] W. Lu, D. Yu, and R. G. Harrison, Phys. Rev. A **58**, R809 (1998).
[17] P. Suret, D. Derozier, M. Lefranc, J. Zemmouri, and S. Bielawski, Phys. Rev. A **61**, 021805 (2000).
[18] R. FitzHugh, Biophys. J. **1**, 445 (1961).
[19] J. S. Nagumo, S. Arimoto, and S. Yoshizawa, Proc. IRE **50**, 2061 (1962).
[20] X. Huang, A. Stintz, H. Li, A. Rice, G. Liu, L. Lester, J. Cheng, and M. Malloy, IEEE J. Quantum Electron. **37**, 414 (2001).
[21] M. Feng, S. Cundiff, R. Mirin, and K. Silverman, IEEE J. Quantum Electron. **46**, 951 (2010).
[22] H. Kawaguchi, *Bistabilities and Nonlinearities in Laser Diodes* (Artech House Publishers, Boston, London, 1994).
[23] M. Giudici, L. Giuggioli, C. Green, and J. R. Tredicce, Chaos Solitons Fractals **10**, 811 (1999).
[24] A. Naumenko, N. A. Loiko, M. Sondermann, K. F. Jentsch, and T. Ackemann, Opt. Commun. **259**, 823 (2006).
[25] M. A. Cataluna, E. U. Rafailov, A. D. McRobbie, W. Sibbett, D. A. Livshits, and A. R. Kovsh, IEEE Phot. Tech. Letters **18**, 1500 (2006).
[26] M. A. Cataluna, D. B. Malins, A. Gomez-Iglesias, W. Sibbett, A. Miller, and E. U. Rafailov, Appl. Phys. Lett. **97**, 121110 (2010).
[27] P. Landais, S. A. Lynch, J. O. Gorman, I. Fischer, and W. Elsäßer, IEEE J. Quantum Electron. **42**, 381 (2006).
[28] A. Tierno, Ph.D. thesis (unpublished), University of Strathclyde (2010).
[29] M. Brunstein *et al.*, Opt. Express **17**, 17118 (2009).
[30] S. Adachi., J. Appl. Phys. **58**, R1 (1985).

[31] T. Rossler, R. A. Indik, G. K. Harkness, J. V. Moloney, and C. Z. Ning, Phys. Rev. A **58**, 3279 (1998).
[32] G. Huyet, S. Balle, M. Giudici, C. K. Green, G. Giacomelli, and J. R. Tredicce, Opt. Commun. **149**, 341 (1998).
[33] M. Ahmed and M. Yamada, IEEE J. Quantum Electron. **38**, 682 (2002).
[34] M. Yamada, W. Ishimori, H. Sakaguchi, and M. Ahmed, IEEE J. Quantum Electron. **39**, 1548 (2003).
[35] L. Furfaro, F. Pedaci, M. Giudici, X. Hachair, J. Tredicce, and S. Balle, IEEE J. Quantum Electron. **40**, 1365 (2004).
[36] A. M. Yacomotti, L. Furfaro, X. Hachair, F. Pedaci, M. Giudici, J. R. Tredicce, J. Javaloyes, S. Balle, E. A. Viktorov, and P. Mandel, Phys. Rev. A **69**, 053816 (2004).
[37] Y. Tanguy, J. Houlihan, G. Huyet, E. A. Viktorov, and P. Mandel, Phys. Rev. Lett. **96**, 053902 (2006).
[38] C. H. Henry, IEEE J. Quantum Electron. **18**, 259 (1982).
[39] P. M. Smowton, E. J. Pearce, H. C. Schneider, W. W. Chow, and M. Hopkinson, Appl. Phys. Lett. **81**, 3251 (2002).
[40] Z. Xu, D. Birkedal, M. Juhl, and J. M. Hvam, Appl. Phys. Lett. **85**, 3259 (2004).
[41] C. Ribbat, R. L. Selin, I. Kaiander, F. Hopfer, N. N. Ledentsov, D. Bimberg, A. R. Kovsh, V. M. Ustinov, A. E. Zhukov, and M. V. Maximov, Appl. Phys. Lett. **82**, 952 (2003).
[42] S. Schneider, P. Borri, W. Langbein, U. Woggon, R. L. Sellin, D. Ouyang, and D. Bimberg, IEEE J. Quantum Electron. **40**, 1423 (2004).
[43] S. P. Hegarty, B. Corbett, J. G. McInerney, and G. Huyet, Electron. Lett. **41**, 416 (2005).
[44] H. C. Schneider, W. W. Chow, and S. W. Koch, Phys. Rev. B **66**, 041310 (2002).
[45] P. Zorabedian, W. Trutna, and L. Cutler, IEEE J. Quantum Electron. **23**, 1855 (1987).
[46] C. Yan, X. Wang, and J. G. McInerney, IEEE J. Quantum Electron. **32**, 813 (1996).
[47] A. P. A. Fischer, O. K. Andersen, M. Yousefi, S. Stolte, and D. Lenstra, IEEE J. Quantum Electron. **36**, 375 (2000).